Mon. Not. R. Astron. Soc. **291,** L42–L46 (1997)

Detection by *ISO* of the far-infrared OH maser pumping lines in IRC+10420

R. J. Sylvester,[1] M. J. Barlow,[1] Nguyen-Q-Rieu,[2] X.-W. Liu,[1] C. J. Skinner,[3] R. J. Cohen,[4] T. Lim,[5] P. Cox,[6] Truong-Bach,[2] H. A. Smith[7] and H. J. Habing[8]

[1]*Department of Physics & Astronomy, University College London, Gower Street, London WC1E 6BT*
[2]*Observatoire de Paris, 61 avenue de l'Observatoire, F-75014 Paris, France*
[3]*Space Telescope Science Institute, 3700 San Martin Drive, Baltimore, MD 21218, USA*
[4]*Nuffield Radio Astronomy Laboratories, Jodrell Bank, Macclesfield, Cheshire SK11 9DL*
[5]*The LWS Instrument-Dedicated Team, ISO Science Operations Centre, PO Box 50727, E-28080 Madrid, Spain*
[6]*Institut d'Astrophysique Spatiale, Bât. 120, Université Paris XI, F-01405, Orsay, France*
[7]*Harvard-Smithsonian Center for Astrophysics, 60 Garden Street, Cambridge, MA 02138, USA*
[8]*Sterrewacht Leiden, PO Box 9513, 2300 RA Leiden, the Netherlands*

Accepted 1997 September 1. Received 1997 August 18; in original form 1997 June 25

ABSTRACT

The population inversions which lead to circumstellar hydroxyl (OH) maser emission from cool stars have long been thought to be radiatively pumped. However, the proposed pumping mechanism has not been directly observed before now, because the spectral lines that correspond to the rotational transitions of the pumping cycle lie in the far-infrared, and are unobservable from the ground.

We present *ISO* observations of IRC+10420, obtained with its Short and Long Wavelength Spectrometers (SWS and LWS, respectively). This object is an F-type hypergiant and a strong OH maser source. The SWS spectrum clearly shows the 34.6-μm doublet in absorption, and the ensuing rotational cascade lines at 98.7, 163 and 79 μm are clearly detected in emission in the LWS spectrum. These spectra provide the first direct confirmation of the radiative pumping cycle for circumstellar OH masers.

Key words: masers – circumstellar matter – stars: individual: IRC+10420 – infrared: stars.

1 INTRODUCTION

Intense radio emission from OH molecules was first detected by Weaver et al. (1965) and was soon attributed to maser action (e.g. Weinreb et al. 1965). OH masers were discovered around dusty evolved stars by Wilson & Barrett (1968). A radiative pumping mechanism for masers had been suggested by Shklovsky (1966), and was worked out in detail for OH/IR star masers by Elitzur, Goldreich & Scoville (1976, hereafter EGS). The OH rotational lines involved in this pumping scheme all occur at far-infrared (FIR) wavelengths, between 30 and 200 μm, unobservable from the ground but accessible to *ISO*'s spectrometers.

OH maser sources exhibit emission from transitions within the $J = 3/2$ $^2\Pi_{3/2}$ ground state (Fig. 1). There are three OH maser lines detected in circumstellar envelopes. The 'main lines' (1665 and 1667 MHz) are dominant in envelopes that are optically thin at 10 μm, whereas the 1612-MHz satellite line dominates in optically thick envelopes. To obtain 1612-MHz masing, the expected pathway (see Fig. 1) is as follows. The ground $^2\Pi_{3/2}$ $J = 3/2$ state is excited to the $^2\Pi_{1/2}$ $J = 5/2$ state by absorption of a 34.6-μm photon (produced by dust in the outflow) – the preferred decay from there is to the $^2\Pi_{1/2}$ $J = 3/2$ state, with emission at 98.7 μm. This is followed by decay to the $^2\Pi_{1/2}$ $J = 1/2$ state, with 163.2-μm emission, and finally to the $^2\Pi_{3/2}$ $J = 3/2$ ground state, with emission at 79.2 μm. Similar excitations to the $^2\Pi_{1/2}$ $J = 3/2$ state by 53.3-μm photons can also contribute to the pump. If the transitions to and from the ground state (34.6, 53.3 and 79.2 μm) are optically thick, while those between the excited levels are optically thin, this scheme causes an inversion of the $F = 2/F = 1$ levels of the ground state, leading to 1612-MHz maser action.

The correctness of the EGS scheme has been supported by indirect tests. Werner et al. (1980) made simultaneous measurements of the maser lines at 18 cm and the broad-band FIR flux (using the Kuiper Airborne Observatory) for a number of OH/IR stars, and showed that sufficient FIR photons were available to pump the masers. Harvey et al. (1974) showed that the maser and IR continuum fluxes varied in phase. See Cohen (1989) or Elitzur (1992) for recent reviews of astronomical masers.

Absorption by the Earth's atmosphere makes the pumping transitions inaccessible to ground-based telescopes, and observations of the FIR OH lines in maser sources, which would provide a direct confirmation of the radiative pumping mechanism, had not been made before the launch of the *Infrared Space Observatory* (*ISO*: Kessler et al. 1996).

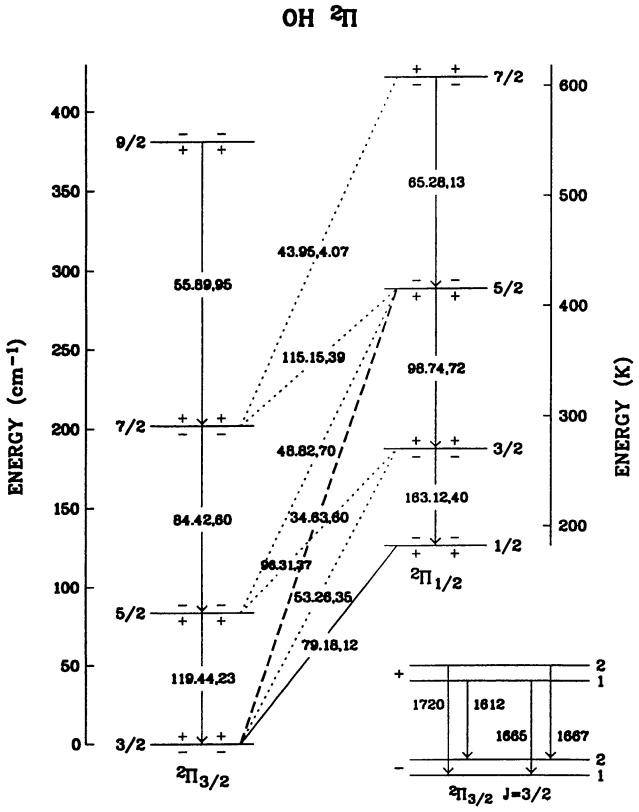

Figure 1. The low-lying energy levels of OH, showing the transitions involved in the maser pumping scheme. The maser action arises from transitions within the $J = 3/2\ ^2\Pi_{3/2}$ ground state.

Skinner et al. (1997) have reported SWS observation of the OH 34.6-μm doublet, in absorption, towards Arp 220, confirming the proposed radiative pumping scheme for this OH megamaser galaxy. Here we report the first observations for a circumstellar OH maser source of both the 34.6-μm OH pumping line and the longer wavelength OH emission lines from the resulting downwards cascade.

1.1 IRC+10420

IRC+10420 (= RAFGL 2390 = V1302 Aql) is a remarkable object. It was classified as an F8 Ia+ hypergiant by Humphreys et al. (1973). There has been some past uncertainty as to whether it is a post-asymptotic giant branch object or a massive supergiant. However, Jones et al. (1993) have made a strong case for it being the latter, with a distance of 4–6 kpc and a luminosity of $\sim 5 \times 10^5\ L_\odot$, putting it near the top of the Hertzsprung–Russell diagram for its effective temperature; we adopt this viewpoint. The object appears to be in a phase of rapid evolution between the M supergiant and Wolf–Rayet stages, and to have increased its temperature by 1000 K in the last 20 years (Jones et al. 1993; Oudmaijer et al. 1996). Strong submillimetre circumstellar CO emission is observed, with an asymmetric line profile; the derived mass-loss rate is very large: around $5 \times 10^{-4}\ M_\odot\ yr^{-1}$ (Oudmaijer et al. 1996).

IRC+10420 is a Type II OH maser source, with the 1612-MHz line stronger than the main lines, although the emission in the latter is still substantial. Strong OH maser emission from IRC+10420 has been observed for over 20 years; over that time, the strength of the 1612-MHz satellite line has steadily increased, while that of the 1667-MHz main line has decreased (Nedoluha & Bowers 1992, and references therein). This is unusual, since for most Type II OH maser sources, the main and satellite lines vary in the same way, in phase with variations in the IR flux. The F-type spectral classification makes it one of the warmest known OH maser stars (Giguere, Woolf & Webber 1976). Nedoluha & Bowers showed that the positions and velocities of the maser spots were inconsistent with the standard model of a thin expanding spherical shell, and modelled the shell of maser-emitting regions as an oblate spheroid with a semi-major axis of 8700 au, with the near side of the equatorial plane tilted 25° above the line of sight and the outflow velocity increasing from 28 $km\,s^{-1}$ in the equatorial plane to 63 $km\,s^{-1}$ along the polar axis.

2 OBSERVATIONS

The observations presented here were all made as part of LWS and Mission Scientist Guaranteed Time. Table 1 summarizes the different observing modes that were used. In this paper, we deal only with the grating spectra; Fabry–Perot spectra which were also obtained will be analysed in a future paper.

2.1 SWS spectra

We obtained SWS grating observations of the 34.6-μm OH pumping line with two different astronomical observation templates (AOTs). In each case, version 5.0 of the data reduction pipeline was used, and the resulting data were reduced with the ISAP package. Details of the SWS instrument and its performance are given by de Graauw et al. (1996), Schaeidt et al. (1996) and Valentijn et al. (1996).

Each of the two SWS grating observations consisted of two scans (one forward, one backward) which were treated separately. Each scan gave 12 subspectra, one per detector. Highly discrepant points caused by cosmic ray hits were removed manually from the subspectra. The subspectra were then scaled to the same flux level to correct for the different responsivities of the detectors. Because the detectors are spaced along the dispersion direction, their resulting subspectra have different (but overlapping) wavelength grids. The subspectra were therefore rebinned to a common

Table 1. Log of *ISO* observations.

AOT[1]	λ (μm)	R[2]	Revolution[3]	Description	On-Target Time
LWS01	43–197	130–320	316	Full grating spectrum	1319 s
SWS06	29–45	900	316	Grating spectrum	1929 s
SWS02	34.35–34.90	1600	364	Grating line scan	295 s

Notes: (1) astronomical observing template; (2) resolving power; (3) orbit number (days) since launch of *ISO* on 1995 November 17.

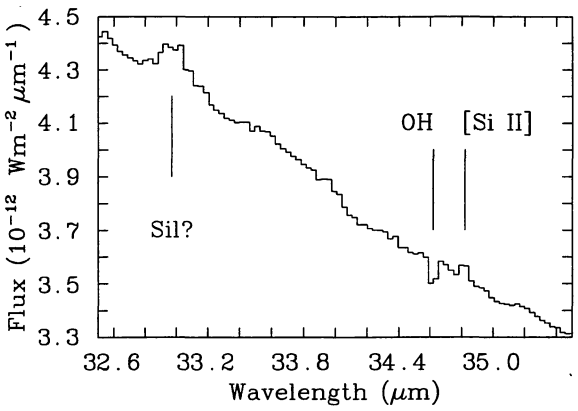

Figure 2. The SWS06 spectrum around 34 μm. The OH 34.6-μm line is clearly seen in absorption, while the [Si II] 34.8-μm line is seen in emission. There is a possible silicate dust emission feature at 33 μm (see Waters et al. 1996 for observations of this feature in other sources).

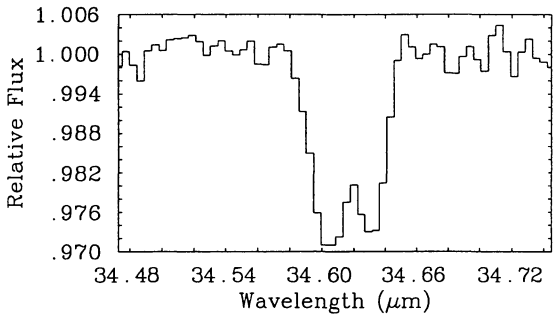

Figure 3. The rectified SWS02 spectrum. The OH 34.6-μm line is resolved into its doublet components (rest wavelengths 34.6035 and 34.6294 μm).

wavelength grid. They were then averaged together, using median clipping to discard points that lay more than 3σ from the median flux. As there was a slight offset between the SWS06 and LWS01 continuum flux levels in their region of overlap (43–45 μm), the SWS06 spectrum was scaled by a factor of 0.89 to obtain agreement. The overall accuracy of the absolute continuum flux levels therefore rests on the LWS calibration. The part of the SWS06 spectrum around the 34.6-μm OH pumping line is presented in Fig. 2.

The two scans of the SWS02 line spectrum gave substantially different continuum shapes, with the forward scan showing a strong rise in the continuum towards long wavelengths. This is probably due to the large change in illumination from the dark current measurement, taken at the start of the observation, to the strong (~1500 Jy) source; this is known to cause hysteresis in the Band 4 detectors (Schaeidt et al. 1996). The scans were therefore rectified before combining them – this averaged spectrum is presented in Fig. 3.

2.2 LWS spectra

All of the downward cascade emission lines in the OH radiative pumping scheme lie in the wavelength region covered by the *ISO* LWS. Details of the instrument and its performance can be found in Clegg et al. (1996) and Swinyard et al. (1996) respectively. We obtained a 43–197 μm grating scan using the LWS01 AOT. The resolution element was 0.3 μm for the the short-wavelength detectors ($\lambda \leq 93$ μm) and 0.6 μm for the long-wavelength detectors ($\lambda \geq 80$ μm). Four samples were taken per resolution element. Six fast grating scans were made, with 0.5-s integrations at each point. An off-source spectrum was taken, at a position 7.2 arcmin from IRC+10420, to enable the Galactic background FIR emission to be subtracted from the on-source spectrum. The same observing

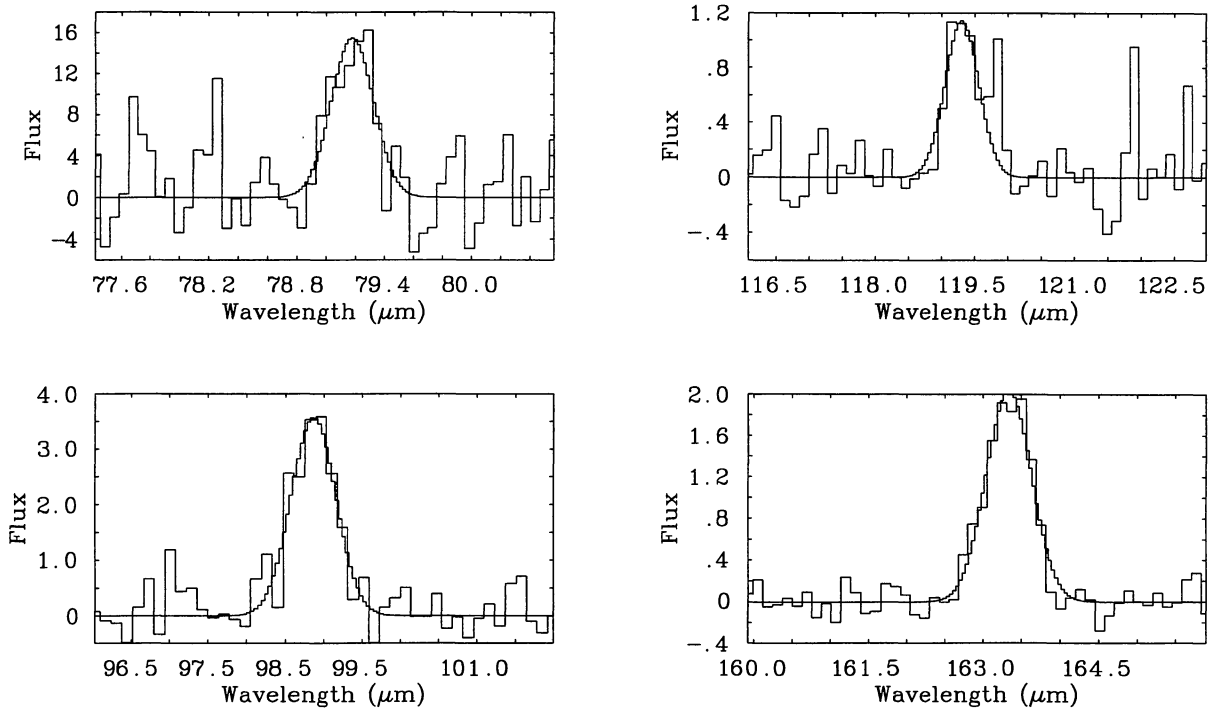

Figure 4. The four detected OH emission lines in the LWS domain (rest wavelengths 79.2, 98.7, 119.3 and 163.2 μm). The units of flux are 10^{-15} Wm^{-2} μm^{-1}. In each plot the underlying continuum has been subtracted.

parameters were used as for the on-source spectrum. The Galactic background flux levels were only significant for $\lambda \geq 100$ μm.

The data were reduced using the LWS off-line processing software (version 6.0), and then averaging the scans using a kappa–sigma algorithm to remove the discrepant points caused by cosmic ray hits. This gave 10 subspectra (one per detector), which were then rescaled to give the same flux in regions of overlap, and merged to give a final spectrum. Detectors SW2 and SW3 are the most photometrically reliable, and were assumed to give a true measure of the source flux; the other detector subspectra required rescaling by less than 20 per cent.

The off-source spectrum is rather noisy, and so was smoothed (apart from the strong 158-μm line) to avoid introducing extraneous noise into the on–off spectrum. In practice, it was found that scaling up the off spectrum by 1.5 and then subtracting it cancelled out the 158-μm line, and also removed an inflection in the continuum at ~150 μm. Continuum-subtracted spectra of the detected OH emission lines are presented in Fig. 4.

3 RESULTS AND DISCUSSION

The measured integrated fluxes (in $\mathrm{W\,m^{-2}}$ and photon $\mathrm{m^{-2}\,s^{-1}}$, a quantity proportional to the rate at which the transitions take place) are presented in Table 2. Upper limits (3σ) are presented for the lines that were not detected.

The 34.6-μm absorption line and the emission lines in the resulting cascade (98.7, 163.2 and 79.2 μm) are all clearly detected in the SWS and LWS spectra, confirming that the EGS radiative pumping cycle does indeed operate. Additionally, the 119.3-μm OH doublet is seen in emission. This transition may well be collisionally excited: it has the largest cross-section amongst the FIR OH transitions for excitation by H_2 collisions (Offer & van Dishoeck 1992).

Maser emission is strongly beamed and is observed in discrete spots, but the same amount of emission should be observed from any viewing angle (from the ensemble of maser spots), so that the emission is globally isotropic. The model of EGS required that, in order to obtain the necessary degree of inversion within the ground $^2\Pi_{3/2}(J = 3/2)$ state, transitions between this state and excited $^2\Pi_{1/2}$ rotational states should be optically thick while transitions between excited $^2\Pi_{1/2}$ levels should be optically thin. The equivalent width that we measure for the 34.6-μm $^2\Pi_{1/2}(5/2) - {}^2\Pi_{3/2}(3/2)$ doublet is 1.33×10^{-3} μm, which for a saturated feature would correspond to a full velocity extent of 11.5 $\mathrm{km\,s^{-1}}$, or 6 $\mathrm{km\,s^{-1}}$ per doublet component. Since each doublet component consists of three hyperfine components (see e.g. fig. 9a of Collison & Nedoluha 1994), the saturated velocity extent of each hyperfine component is therefore about 2 $\mathrm{km\,s^{-1}}$, about a factor of 2 larger than the linewidths predicted for weaker, lower velocity Mira winds in the modelling of Collison & Nedoluha (1994; their fig. 9a). The 53.3- and 79.2-μm $^2\Pi_{1/2} - {}^2\Pi_{3/2}$ transitions, and the 119.3-μm $^2\Pi_{3/2}(5/2) - {}^2\Pi_{3/2}(3/2)$ transition, all have higher Einstein B-coefficients than that of the 34.6-μm transition (see e.g. fig. 5 of Collison & Nedoluha 1993), and hence they too will all be optically thick. Since the number Φ of photons absorbed per unit area per unit time in an optically thick velocity range δv is given by

$$\Phi = (F_\nu/h\nu) \times (\delta v/c)\nu \propto F_\nu,$$

where the symbols have their usual meanings, we can use the observed photon absorption rate in the 34.6-μm transition of $83\times10^4\ \mathrm{m^{-2}\,s^{-1}}$ and the observed relative continuum fluxes at the relevant wavelengths to predict the absorption rates in the other transitions connecting to the ground state.

From our SWS and LWS spectra we measure continuum flux densities of 1438 Jy at 34.6 μm and 824, 393 and 130 Jy at 53.3, 79.2 and 119.3 μm, which imply photon absorption rates of 48×10^4, 23×10^4 and $7.5\times10^4\ \mathrm{m^{-2}\,s^{-1}}$, respectively. The latter rate is much smaller than the observed *emission* rate of $43\times10^4\ \mathrm{m^{-2}\,s^{-1}}$ in the 119.3-μm transition (Table 2), confirming that the observed line must be collisionally excited. The predicted photon absorption rates in the 53.3- and 79.2-μm lines are respectively 57 and 27 per cent of that in the 34.6-μm line, so that the former two lines cannot be neglected in overall pump efficiency estimates. The detailed modelling of Collison & Nedoluha (1994) predicts that the 53.3-μm transition should be in net absorption, with a small amount of emission infilling (their fig. 9b), so our observed 3σ upper limit of $43\times10^4\ \mathrm{m^{-2}\,s^{-1}}$ for the *net* 53.3-μm photon absorption rate (Table 2) is consistent with the absorption rate of $48\times10^4\ \mathrm{m^{-2}\,s^{-1}}$ predicted above by scaling from the observed 34.6-μm photon absorption rate.

From Fig. 1, the downward photon emission rate in the 98.7-μm transition should be equal to the upward absorption rate in the 34.6-μm transition. The observed rates of $(130\pm20)\times10^4\ \mathrm{m^{-2}\,s^{-1}}$ and $(83\pm8)\times10^4\ \mathrm{m^{-2}\,s^{-1}}$, respectively, are consistent with each other within their 2σ errors. Also from Fig. 1, the observed downward rate in the 163.2-μm transition of $(120\pm16)\times10^4\ \mathrm{m^{-2}\,s^{-1}}$ should be equal to the sum of the upward rates in the 34.6- and 53.3-μm transitions, i.e. $(83+43 = 126\pm16)\times10^4\ \mathrm{m^{-2}\,s^{-1}}$. The 53.3-μm absorption rate should be apparent as an excess photon rate in the 163.2-μm line compared with the 98.7-μm line. However, this excess is not detected in the data: we obtain only a 3σ upper limit of $65\times10^4\ \mathrm{m^{-2}\,s^{-1}}$ for the difference between the 163.2- and 98.7-μm photon rates.

The downward cascade rate should also contribute to the 79.2-μm transition to the ground rotational state, augmented by collisional excitation of this line from the ground state. Since the collisional excitation rates calculated for 100 and 600 K for the 79.2-μm transition by Offer & van Dishoeck (1992; their table 6) are both about two-thirds of those for the 119.3-μm transition, we can use the 119.3-μm photon rate of $(43\pm9)\times10^4\ \mathrm{m^{-2}\,s^{-1}}$ to predict a 79.2-μm collisional rate of $(29\pm6)\times10^4\ \mathrm{m^{-2}\,s^{-1}}$ and hence a total emission rate of $(130+29 = 159\pm21)\times10^4\ \mathrm{m^{-2}\,s^{-1}}$ in the 79.2-μm line. The observed 79.2-μm emission rate of $(200\pm30)\times10^4\ \mathrm{m^{-2}\,s^{-1}}$ is consistent with this total predicted emission rate for cascades from higher levels, plus collisional excitation from the ground

Table 2. Measured line strengths and photon rates from grating spectra, with 1σ uncertainties. Units of integrated flux and photon rate are $10^{-15}\ \mathrm{W\,m^{-2}}$ and $10^4\ \mathrm{m^{-2}s^{-1}}$ respectively.

λ (μm)	Transition (J value in parentheses)	Integrated Flux	Photon rate
34.6	$^2\Pi_{1/2}(5/2) - {}^2\Pi_{3/2}(3/2)$	−4.8±0.4	83±8
48.8	$^2\Pi_{1/2}(5/2) - {}^2\Pi_{3/2}(5/2)$	<15	<370
53.3	$^2\Pi_{1/2}(3/2) - {}^2\Pi_{3/2}(3/2)$	<1.6	<43
79.2	$^2\Pi_{1/2}(1/2) - {}^2\Pi_{3/2}(3/2)$	5.2±0.8	200±30
84.5	$^2\Pi_{3/2}(7/2) - {}^2\Pi_{3/2}(5/2)$	<1	<42
96.3	$^2\Pi_{1/2}(3/2) - {}^2\Pi_{3/2}(5/2)$	<1	<50
98.7	$^2\Pi_{1/2}(5/2) - {}^2\Pi_{1/2}(3/2)$	2.6±0.4	130±20
119.3	$^2\Pi_{3/2}(5/2) - {}^2\Pi_{3/2}(3/2)$	0.73±0.15	43±9
163.2	$^2\Pi_{1/2}(3/2) - {}^2\Pi_{1/2}(1/2)$	1.5±0.2	120±16
1612-MHz	$^2\Pi_{3/2}(3/2)\ F{=}1^+{\rightarrow}2^-$	6.6×10^{-5}	6.2

state. The ground state population inversion requires downwards 79.2-μm transitions. Thus, for comparison with the 1612-MHz photon rate, the observed *net* 79.2-μm rate should be corrected for a predicted diminution of $23\times10^4\,m^{-2}\,s^{-1}$ by an unresolved absorption component, implying a photon rate for the emission component of $(223 \pm 32)\times10^4\,m^{-2}\,s^{-1}$.

4 PUMPING EFFICIENCY

The integrated flux of IRC+10420 in the 1612-MHz maser line as measured with the Nancay radio telescope on 1996 October 17 (mid-way between our *ISO* observations on Revs. 316 and 364) was 6.2×10^4 photon $m^{-2}\,s^{-1}$. We can define a pumping efficiency as the number of maser photons emitted per molecule undergoing the pumping cycle, i.e. the ratio of the photon emission rate in the radio maser line to that in the 79.2-μm pump line (Fig. 1). From the present observations, this ratio is 2.8 per cent.

A definition of the OH maser efficiency used in the past was simply the ratio of the peak 1612-MHz flux density to the 34.6-μm continuum flux density. This compares the maser output with the potentially available pumping photons. For IRC+10420, the 34.6-μm continuum flux of 1438 Jy from the SWS06 spectrum and the peak 1612-MHz flux density of 73 Jy (taking an average of the fluxes of the low- and high-velocity peaks) give an efficiency of 5.2 per cent, similar to the median value derived by Dickinson (1991) for a group of 50 maser stars with *IRAS* continuum flux ratios similar to those of IRC+10420. However, if we take into account the extra pumping photons contributed by absorption in the 53.3- and 79.2-μm lines (derived above to amount to 80 per cent of those contributed by the 34.6-μm line), the pumping efficiency decreases to 3 per cent, in agreement with the pumping efficiency estimated from the integrated emission rates in the 1612-MHz and 79.2-μm lines. Since velocity overlap between far-infrared line subcomponents can also lead to ground state inversion, particularly in the main lines (Litvak 1969; Bujarrabal et al. 1980; Collison & Nedoluha 1993), our estimate of 3 per cent for the pump efficiency probably represents an upper limit. OH pumping by near-infrared photons (Bujarrabal et al. 1980; Collison & Nedoluha 1994) is probably not significant for IRC+10420 because of the reduction of its near-infrared continuum flux by circumstellar dust absorption. Maser efficiency has also been considered in terms of the energy flux in the maser lines and in the 34.6-μm absorption line. The ratio of these gives an 'energy efficiency' of 1.4×10^{-5}.

ACKNOWLEDGMENTS

We thank Eric Gerard at Nancay for obtaining the radio observations for us. This work made use of the SIMBAD data base, provided by the CDS, Strasbourg. We thank the referee, Dr M. Elitzur, for useful comments. This paper was based on observations with *ISO*, an ESA project with instruments funded by ESA Member States (especially the PI countries: France, Germany, the Netherlands and the United Kingdom) with the participation of ISAS and NASA.

REFERENCES

Bujarrabal V., Guibert J., Nguyen-Q-Rieu, Omont A., 1980, A&A, 84, 311
Clegg P. E. et al., 1996, A&A, 315, L38
Cohen R. J., 1989, Rep. Prog. Phys., 52, 881
Collison A. J., Nedoluha G. E., 1993, ApJ, 413, 735
Collison A. J., Nedoluha G. E., 1994, ApJ, 422, 193
de Graauw Th. et al., 1996, A&A, 315, L49
Dickinson D. F., 1991, ApJ, 379, L29
Elitzur M., 1992, Astronomical Masers. Kluwer, Dordrecht
Elitzur M., Goldreich P., Scoville N., 1976, ApJ, 205, 384 (EGS)
Giguere P. T., Woolf N. J., Webber J. C., 1976, ApJ, 207, L195
Harvey P. M., Bechis K. B., Wilson W. J., Ball J. S., 1974, ApJS, 27, 331
Humphreys R.M., Strecker D.W., Murdock T.L., Low F.J., 1973, ApJ, 179, L53
Jones T. J. et al., 1993, ApJ, 411, 323
Kessler M. F. et al., 1996, A&A, 315, L27
Litvak M. M., 1969, ApJ, 156, 471
Nedoluha G. E., Bowers P. F., 1992, ApJ, 392, 249
Offer A. R., van Dishoeck E. F., 1992, MNRAS, 257, 377
Oudmaijer R. D., Groenewegen M. A. T., Matthews H. E., Blommaert J. A. D. L., Sahu K. C., 1996, MNRAS, 280, 1062
Schaeidt S. G. et al., 1996, A&A, 315, L55
Shklovsky I. S., 1966, Astron. Tsirk., No. 372
Skinner C. J., Smith H. A., Sturm E., Barlow M. J., Cohen R. J., Stacey G. J., 1997, Nat, 386, 472
Swinyard B. M. et al., 1996, A&A, 315, L43
Valentijn E. A. et al., 1996, A&A, 315, L60
Waters L. B. F. M. et al., 1996, A&A, 315, L361
Weaver H., Williams D. R. W., Dieter N. H., Lum W. T., 1965, Nat, 208, 29
Weinreb S., Meeks M. L., Carter J. C., Barrett A. H., Rogers A. E. E., 1965, Nat, 208, 440
Werner M. W., Beckwith S., Gatley I., Sellgren K., Berriman G., Whiting D. L., 1980, ApJ, 239, 540
Wilson W. J., Barrett A. H., 1968, Sci, 161, 778

This paper has been typeset from a TEX/LATEX file prepared by the author.